Issues in Frequency Analysis of δ Scuti Stars II—EE Cha (HD 104036)

Bill Rea
Richmond, New Zealand; rea.william@gmail.com

Received January 22, 2022; revised April 18, 2022; accepted May 12, 2022

Abstract Pre-whitening is a commonly used procedure in the frequency analysis of variable star light curves when multiple pulsation frequencies are active. However, each pre-whitening cycle introduces a new frequency into the data, often resulting in statistically significant frequencies appearing in the analysis which do not correspond to a pulsation within the star. In this paper we examine the effectiveness of a simple modification, permitted by some frequency analysis software packages, which we call restricted range analysis. We show that while restricted range analysis may considerably reduce the number of spurious frequencies generated it does not eliminate them. Thus each reported significant frequency must still be checked against the periodogram to confirm it matches a clear feature within it. Further, restricted range analysis appears to not detect some frequencies and these must be searched for in the periodogram. We conclude that while restricted range analysis is useful, it does not overcome all the problems associated with pre-whitening in frequency analysis.

1. Introduction

In the previous paper (Rea 2022), which we will refer to as Paper I, we set out for the amateur variable star observing community some issues which commonly arise in the analysis of stars with multiple pulsation modes excited, particularly focusing on δ Scutis. While some solutions have been proposed in the professional literature (see, for example, Lares-Maritz *et al.* (2020)), often there are no freely available software packages which implement these new methods.

In Paper I we proposed a simple modification to the standard methods of frequency analysis which can be implemented in some existing software packages and which we termed "restricted range analysis." The modification was aimed at reducing the often very large number of spurious frequencies arising from the use of pre-whitening. EE Cha appears to be an interesting case to study both because of its young age and its periodogram appears to be quite simple in structure (see below). This simple periodogram structure should make the analysis of its pulsation frequencies easier than for a star with a more complicated pulsation structure. In this paper we seek to evaluate in some detail the strengths and weaknesses of restricted range analysis using EE Cha as a test case.

1.1. EE Cha and asteroseismology

EE Cha (HD 104036) is a deeply southern δ Scuti variable which, like many other southern δ Scutis, has been little studied. It is part of the ε Cha association of very young (4–10 Myr) stars in the solar neighborhood, some of which still exhibit proto-planetary disks (Murphy *et al.* 2013), although EE Cha itself has not been reported to have such a disk. It was discovered by Kurtz and Müller (1999) who reported two periods in their data of 33.88 cycles d^{-1} and 29.31 cycles d^{-1}. Table 1 presents some parameter estimates for the star. The data were drawn from the TASOC web site (https://tasoc.dk/), SIMBAD (http://simbad.u-strasbg.fr/simbad/) Wenger et al. (2000), and the Variable Star Index (VSX, https://www.aavso.org/vsx/). The distance is from the Gaia 2020 catalog (Gaia Collab. 2020). The TIC is the TESS Input Catalog number.

Table 1. Basic stellar data for EE Cha/HD 104036.

Property	*Value*
Spectral Type (VSX)	A7V
Period	0.029516 days / 42.503 min
Distance	104.8 ± 0.29 pc
Mean Mag (V)	6.73
Amplitude (B)	0.11
TIC	454961439

Because the evolution of main sequence stars is slow, observational tests of theories of stellar evolution must be made by observing a range of similar stars with different ages. EE Cha is of particular interest because it has only recently reached the main sequence. Consequently it is a good candidate to study to understand the earliest phases of a δ Scuti's evolution. Grigahcène *et al.* (2010) report that δ Scutis have a shallower convective envelope than solar-like stars but this slowly deepens as the star ages. It is in this shallow convective zone that the p-mode pulsations originate and propagate. Aerts and Kurtz (2010, p. 52) indicate that for δ Scutis with $M_\star > 2M_\odot$ the outer zone is radiative rather than convective. A shallow convective zone could account for short periods of the p-mode pulsations seen in some δ Scutis. A second consequence of a shallow convective zone is that g-mode pulsations, which form and propagate in the radiative interior, have less material to propagate through to the surface where they can be observed, and hence are less likely to be attenuated to insignificance, such as appears to be the case with solar-like stars.

As reported in Paper I, while δ Scutis are of particular interest for asteroseismology because they often exhibit both p- and g-mode pulsations, a significant obstacle has been identifying the often many active pulsation modes in any given star. Balona (2014) showed that the commonly used technique of pre-whitening time series data during frequency analysis introduces a new frequency into the data with each pre-whitening cycle. This was sufficiently problematic that in numerical experiments numerous spurious frequencies were identified as statistically significant, while some real frequencies

in his simulated data were not identified. The simulated data used by Balona (2014) met the three assumptions which are made when pre-whitening is used, that is: (1) the frequencies were generated by sinusoids; (2) they were stationary in both amplitude and frequency; and (3) they were combined into the final light curve in an additive manner. Paper I extended the work of Balona (2014) and investigated the effect of violations of these three assumptions on frequency analysis using pre-whitening, and concluded that the number of statistically significant but entirely spurious frequencies is likely to be much higher than in the ideal case.

Given that in the literature on δ Scutis sometimes hundreds of significant frequencies are reported (Poretti *et al.* 2009; Uytterhoeven *et al.* 2011) requiring hundreds of pre-whitening cycles in the frequency analysis, it is likely that many reported frequencies are an artifact of the method of analysis and do not correspond to any physically meaningful pulsation.

The remainder of the paper is structured as follows: section 2 discusses the numerical experiments and their results; section 3 discusses the data for EE Cha and the analysis methods; section 4 presents the results; section 5 contains the discussion; and section 6 gives our conclusions.

2. Numerical experiments

While the generation of a number of simulated data sets was discussed in Paper I, none of those were particularly suited to testing restricted range analysis. Consequently, a new data set was generated consisting of 18 frequencies in six groups of three frequencies; details are given in Table 2.

While the units of the simulated data were in arbitrary units, they were chosen to mimic the data from NASA's Transiting Exoplanet Survey Satellite (TESS) (Ricker *et al.* 2014) in its 120-second cadence observing mode. There were six groups of triplets with a central frequency and two side frequencies at a spacing of 0.5 cycle d^{-1}. Three sets, or nine frequencies, were sinusoids, namely "δ Scuti low 1," "δ Scuti high 1," and "δ Scuti high 3." In the first group, the "γ Dor" frequencies, the amplitudes of the sinusoids were modulated by a second sinusoid through four cycles over the length of the time series. In the third group, the "δ Scuti low 2" group, the amplitude was constant over the first quarter of the data, then reduced by a factor of one-half over the next quarter, and then remained constant to the end of the series. In the fifth group, the "δ Scuti high 2" group, the amplitude was modulated with a slow rise followed by a rapid decrease in a ratio of 3:1. There were eight complete cycles over the course of the data. Finally the data were summed, standardized to an amplitude 1 (again in arbitrary units), and noise added of 0.001 of the amplitude of the final series. There were 131,072 data points in the final series. The periodogram of the data is presented in Figure 1 in black.

The data were then subjected to both an unrestricted range analysis and an eight-stage restricted range analysis. The results from these two analyses are presented in Table 3, The second column of which reports the actual number of frequencies present in the data for that frequency range. The periodogram of the residuals from the eight stage restricted range analysis is in red in Figure 1.

Table 2. The frequencies and their properties which were used to construct the simulated light curve.

Frequency Group	*Frequency*	*Amplitude Range*
γ Dor	1.5	0.125–0.375
Amplitude	2.0	0.250–0.750
Modulation	2.5	0.125–0.375
δ Scuti low 1	8.5	0.500
Sinusoids	9.0	1.000
	9.5	0.500
δ Scuti low 2	11.5	0.250–0.500
Amplitude	12.0	0.500–1.000
Reduction	12.5	0.250–0.500
δ Scuti high 1	17.5	0.500
Sinusoids	18.0	1.000
	18.5	0.500
δ Scuti high 2	21.5	0.250–0.750
Slow rise	22.0	0.500–1.500
Rapid fall	22.5	0.250–0.750
δ Scuti high 3	31.5	0.500
Sinusoids	32.0	1.000
	32.5	0.500

Table 3. The number of statistically significant frequencies reported by SigSpec (Reegen 2011) in both the eight stage restricted range analysis and the unrestricted analysis.

Frequency Range Cycles d^{-1}	*Real Frequencies*	*No. Significant Restricted*	*Frequencies Unrestricted*
0.0–3.0	3	9	9
3.0–8.0	0	0	0
8.0–13.0	6	13	16
13.0–17.0	0	0	0
17.0–23.0	6	20	26
23.0–31.0	0	0	0
31.0–33.0	3	3	3
33.0–50.0	0	0	0
Total	18	45	54

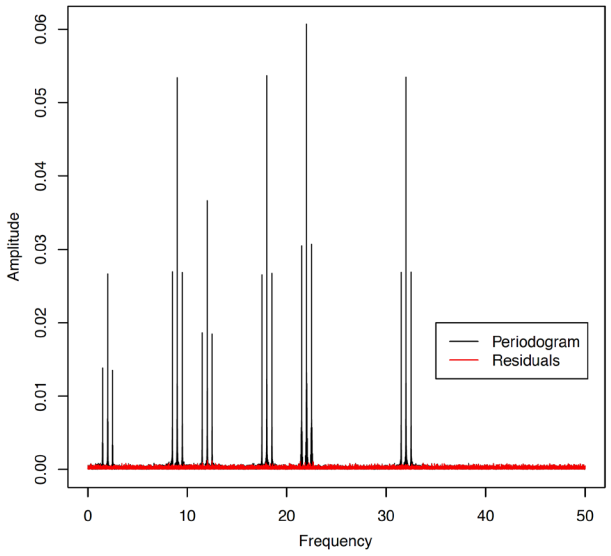

Figure 1. The periodogram of the simulated data set is in black, while the periodogram of the residuals from the eight stage restricted range analysis is in red.

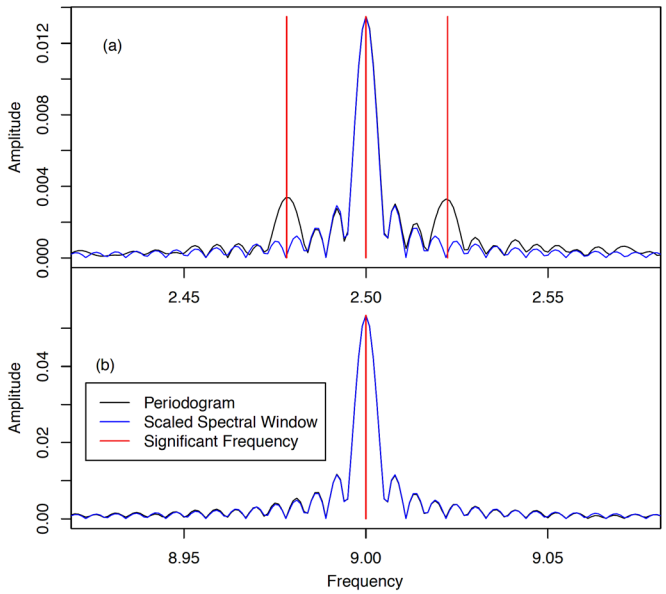

Figure 2. The periodogram simulated data set near the frequencies 2.5 (panel a) and 9.0 (panel b) cycles d^{-1}. The locations of the statistically significant frequencies are marked in red. The two frequencies on either side of the peak at 2.5 cycles d^{-1} were not present in the data and so are examples of spurious frequencies.

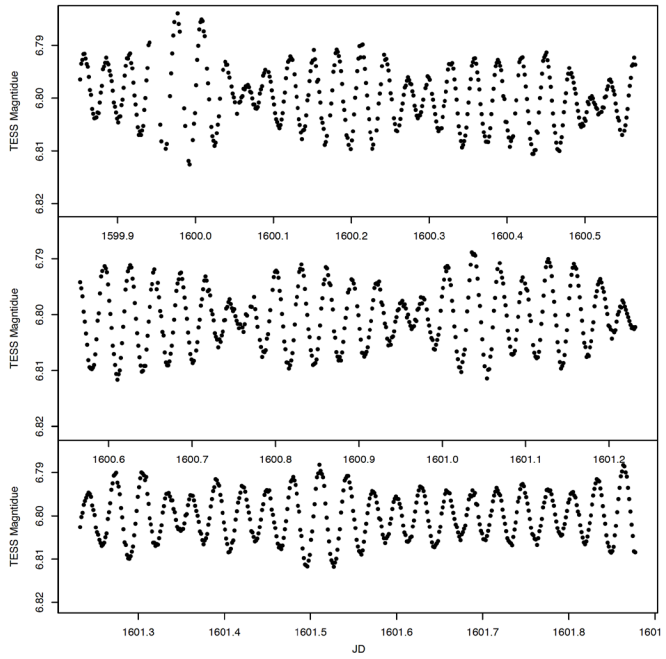

Figure 3. Approximately two days of TESS data for EE Cha (HD 104036). The units of the horizontal axis are barycentric Julian days –2457000.

Two examples of small portions of the periodogram are presented in Figure 2, in which spurious frequencies were (panel a) and were not (panel b) reported.

3. Data and analysis methods

At the initiation of this study EE Cha had no observations available in the AAVSO's International Database. However, EE Cha was observed by NASA's TESS in Sectors 11 and 12 of its mission in its two-minute cadence mode. The raw data for this paper were downloaded from the TESS Asteroseismic Science Operations Center (TASOC) web site on 09 January 2021. They covered a period of approximately 53 days. The reported corrected flux was converted to magnitudes using the value for EE Cha's magnitude in the V band as reported on the TASOC web site as the mean value for each observation run. Observations were discarded if the value in the Pixel Quality Field (PQF) was non-zero or either the date or the corrected flux was recorded as not-a-number (nan). This resulted in 34,070 usable data points. Figure 3 presents an approximately two-day continuous segment of the light curve in which beating between two or more frequencies can clearly be seen. The approximately one-day data gaps caused by the data download from the satellite to the ground do not appear in this Figure.

SigSpec (Reegen 2011), FAMIAS (Zima 2008), and user-written R code (R Core Team 2019) were used to carry out the frequency analysis. FAMIAS was limited to 100 statistically significant frequencies, whereas SigSpec has, for all practical purposes, no upper bound on the number of frequencies which may be reported.

An unrestricted frequency analysis was run using both SigSpec and FAMIAS. The significance cut-off level for SigSpec was set to 4, arguably a low value. The signal-to-noise ratio cut-off level for FAMIAS was also 4. The total numbers of significant frequencies and their types from these two analyses are given in Table 6 below.

A restricted range analysis was also carried out using SigSpec, again setting the cut-off significance level to 4. SigSpec has two keyword directives, lfreq and ufreq, which allow the user to set the lowest and highest frequencies to be included in frequency analysis with frequencies outside this range being excluded. Based on an inspection of the periodogram, the 0 to 75 cycles d^{-1} frequency range was split into nine sub-ranges, the details of these ranges are given in Table 4. As can be seen in the Table there are some small overlaps in some of these ranges. The guiding principle was to try to restrict the ranges to blocks where either significant frequencies could be visually identified or the range appeared to consist of nothing but noise. For example, the range 0.28–3.2 cycles d^{-1} contained two frequencies which could easily be identified by visual inspection, while the ranges on either side, namely 0.0–0.3 and 3.0-20.0 cycles d^{-1}, appeared to contain only noise.

Table 4. The frequency ranges used in the restricted range analysis together with the number of statistically significant frequencies reported.

Frequency Range	*Significant Frequencies*
0.0–0.3	0
0.28–3.2	2
3.0–20.0	0
20–25	2
25–30	11
30–35	16
35–40	0
40–60	0
60–75	1
Total	32

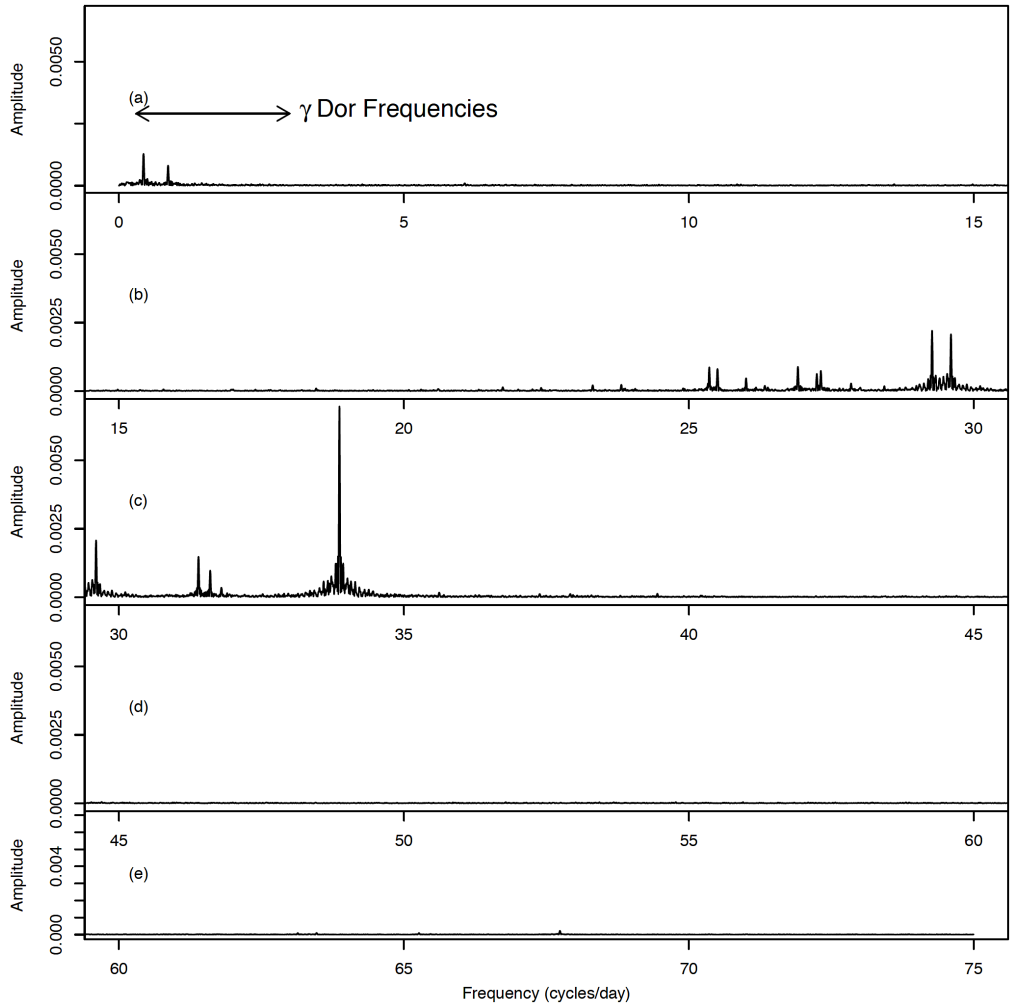

Figure 4. The Fourier periodogram of the complete TESS data for EE Cha (HD 104036) obtained using FAMIAS (Zima 2008). The five panels break the periodogram into 15 cycles d^{-1} segments with panel (a) covering the 0–15 cycles d^{-1} range, through to panel (e), which covers the 60–75 cycles d^{-1} range. The range of frequencies corresponding to the γ Doradus g-mode frequency range is marked in panel (a).

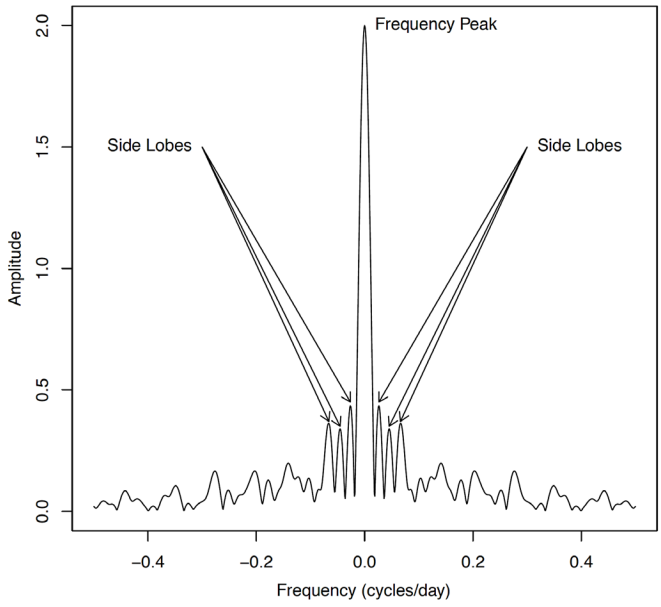

Figure 5. The spectral window of the complete TESS data obtained using FAMIAS (Zima 2008). The central peak has three clear side lobes.

Table 5. The frequency spacing and the relative height of the three main side lobes of the spectral window plotted in Figure 5. The height of the central frequency peak is normalised to one.

Side Lobe	*Frequency Spacing (cycles d^{-1})*	*Relative Height*
1	0.026404	0.2174
2	0.045264	0.1701
3	0.066010	0.1814

Table 6. The number of different types of statistically significant frequencies in the combined data set as reported by SigSpec (Reegen 2011), FAMIAS (Zima 2008) and using a restricted range analysis with SigSpec as described in the text.

Frequency Type	*SigSpec*	*FAMIAS*	*Restricted Range*
δ Scuti	479	82	30
γ Dor	60	7	2
Others	10	9	0
Total	549	98	32

The ranges in Table 4 were analyzed by SigSpec and the residuals from each lower frequency range were used as input into the next higher range. For example, the residuals from the 0.0–0.3 cycle d^{-1} range were used in the frequency analysis of the 0.28–3.2 cycles d^{-1} range, the residuals of which were then used in the 3.0–20.0 cycles d^{-1} range. The purpose of using the residuals rather than the original data set was two-fold. First, once all nine frequency ranges had been successively analyzed, the final set of residuals could be used to generate a periodogram for comparison against the original periodogram of the data set. Secondly, it was clear from initial investigations that sometimes a high peak in the periodogram outside the restricted frequency range being analyzed was either noticeably lowered or reduced to the level of the noise. The alternative, of using the original data set for each restricted range, was not investigated in detail so could perhaps be studied later.

User-written R code (R Core Team 2019) was used to plot each statistically significant frequency against the periodogram. The spectral window, generated by either SigSpec or FAMIAS as appropriate, was scaled by the height (amplitude) of the significant frequency and overplotted on the periodogram. A visual inspection was carried out to check if the identified statistically significant frequency matched an identifiable feature in the periodogram.

4. Results

Both FAMIAS (Zima 2008) and SigSpec (Reegen 2011) were used to obtain a periodogram of the data. Figure 4 plots the periodogram obtained using FAMIAS out to 75 cycles d^{-1}, which covers the range within which statistically significant frequencies were obtained. The highest significant frequency was 67.738957 cycles d^{-1}. In panel (a) of Figure 4 the range of g-mode frequencies, also known as γ Doradus frequencies, is marked. All other higher frequencies were considered to be p-mode or δ Scuti frequencies.

The TESS data had significant gaps caused by the operational requirements resulting from its 13.7-day orbital period. Data gaps can give rise to the presence of aliases which must be taken account of during any frequency analysis. Figure 5 presents a plot of the spectral window, which is the Fourier transform of a noiseless sinusoid sampled in the same way as the data; see Aerts and Kurtz (2010) section 5.3.3 for more details on the spectral window. Three strong side lobes were visible in the window. They are marked in Figure 5. Details of their frequency deviation from the main peak and their height relative to it after standardizing the peak to a height of one are given in Table 5. The evidence presented in the Figure and a close examination of the numerical data for the spectral window do not indicate a strong alias in the data at the inverse of the orbital period, that is, at (or near) 0.072993 cycle d^{-1}. However, the inverse of the orbital period lies quite close to the third side lobe of the spectral window and it is possible the two have been merged into an apparent single side lobe.

Because FAMIAS was limited to a maximum of 100 statistically significant frequencies a second frequency analysis was carried out using SigSpec (Reegen 2011), and the results from both FAMIAS and SigSpec are presented in Table 6. The ranges of frequencies classified as either δ Scuti or γ Doradus were those of Catelan and Smith (2015) Table 9.1, namely $0.3 \leq f < 3$ were classified as γ Doradus types and $f \geq 3$ cycles d^{-1} were classified as δ Scuti types. The remaining frequencies, for which $f < 0.3$, were classified as other. However, one should note that Grigahcène *et al.* (2010), in their Figure 2, showed that for hybrid γ Doradus/δ Scuti stars the γ Doradus and δ Scuti frequency ranges should not overlap. If we had taken their gap into account, which depends on a precise measure of the effective temperature, some of the frequencies classified as δ Scuti should perhaps be classified as other.

Figure 6 presents a scatter plot of the 549 statistically significant frequencies reported by SigSpec in the order in which they were identified. It is fairly easy to observe the gradual fanning out of frequencies from the two areas of the periodogram with highly significant frequencies, namely the 25–35 cycles d^{-1} and 0.4–0.9 cycle d^{-1} regions, into the adjacent frequency regions.

Of the 32 statistically significant frequency reported by the restricted range analysis, 13 of these had a problem when matched to the periodogram. There were two types of problems: firstly, the identified frequency was close to the local peak of the periodogram but did not match it and, secondly, there was no discernible feature in the periodogram at, or near, the location of the frequency. Examples of both of these problems are presented in Figure 7. The first is illustrated in panel (a) and the second in panel (b).

The periodogram of the residuals from the final stage of the restricted range analysis was plotted against the periodogram of the data to check if there appeared to be any clear peaks which had been missed by the restricted range analysis. A plot of both periodograms appears in Figure 8. From an analysis of the periodogram of the residuals and comparing the remaining peaks with the results of the unrestricted analysis, a further eight significant frequencies were identified; these are reported in Table 7. The frequencies F1 through F22 in Table 7 were

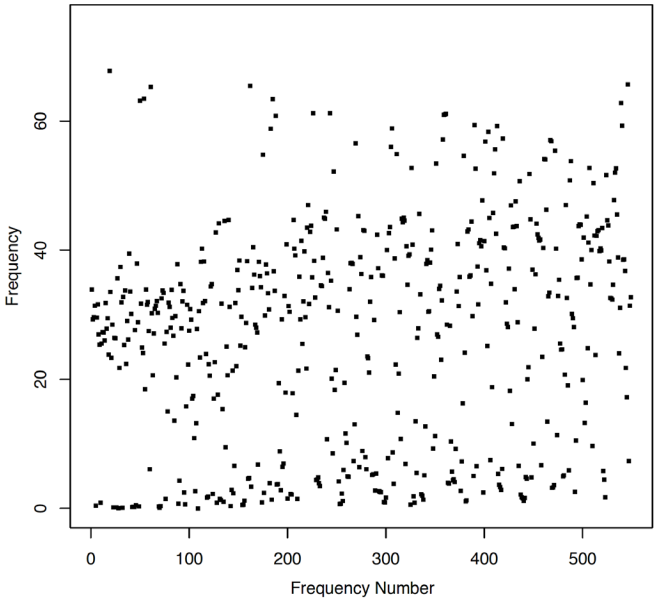

Figure 6. The statistically significant frequencies from the complete TESS data set in the order in which SigSpec (Reegen 2011) reported them.

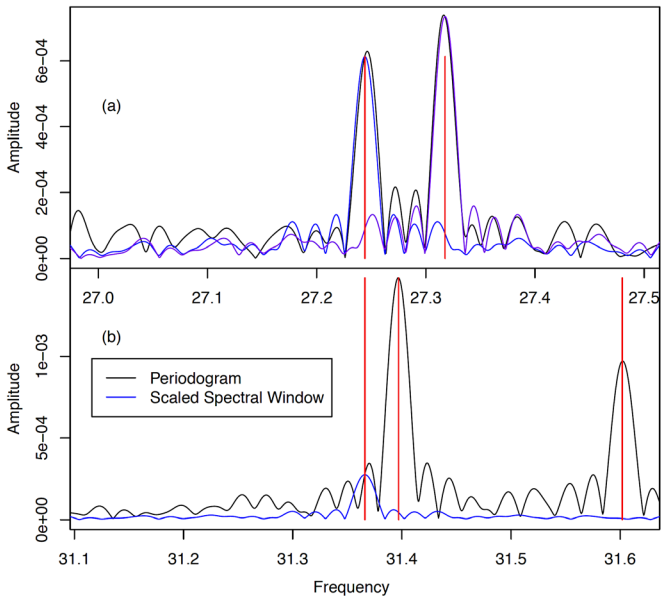

Figure 7. Examples of the two types of problems which arose in the restricted range frequency analysis. In both panels the periodogram is marked in black, the scaled spectral window in blue, and the locations of the significant frequencies in red. Panel (a) is an example of when the identified frequency did not match the location of the local peak in the periodogram. Panel (b) is an example of when the identified frequency could not be matched to any feature in the periodogram.

Table 7. The final list of significant frequencies.

Number	*Frequency*	*SNR*	*Number*	*Frequency*	*SNR*
F1	0.432322	29.19	F16	31.397066	64.55
F2	0.863226	18.86	F17	31.601901	42.91
F3	23.313647	21.40	F19	31.798934	15.23
F4	23.815548	23.65	F19	31.894335	6.57
F5	25.358788	57.76	F20	31.940864	4.45
F6	25.503446	57.41	F21	33.869470	323.41
F7	26.004749	27.95	F22	67.738708	47.92
F8	26.913886	54.10	F23	20.299375	7.15
F9	27.244179	31.67	F24	20.598099	8.48
F10	27.317593	38.04	F25	21.737048	13.68
F11	27.846068	14.32	F26	22.408476	12.18
F12	29.267407	96.72	F27	24.062921	7.47
F13	29.534648	46.91	F28	26.337816	11.29
F14	29.599931	97.35	F29	26.386373	11.20
F15	30.112743	4.87	F30	27.639601	5.44

Table 8. Pairs of frequencies of the form f, 2f.

f_1	$f_2 = 2f_1$	$2f_1 - f_2$	*Amplitude Ratio* f_1 / f_2
0.432322	0.863226	0.001418	1.62
33.869470	67.738708	0.000232	31.53

identified by the restricted range analysis. Frequencies F23 through F30 were identified by visual inspection and comparison of the periodograms of the data and the residuals from the same restricted range analysis. All 30 frequencies were subject to a least squares fit in FAMIAS and the signal-to-noise ratios (SNR) reported in the final column were calculated by FAMIAS.

A search was made for frequency groupings of the form f, 2f, 3f... and only two were found. These are reported in Table 8 in which the third column gives a measure of how exact the 2:1 frequency ratio is. The final column is the ratio of the amplitudes of the two frequencies. A search was also made for regular frequency spacings such as doublets or triplets and two doublets were found. These are plotted in Figure 9.

5. Discussion

5.1. Simulated light curve

For the simulated light curve both the restricted and unrestricted frequency analysis recovered all 18 of the real frequencies. In the periodogram of the simulated light curve in Figure 1 the six sets of three frequencies are easily seen. Thus it is unsurprising that they were all recovered. The periodogram of the residuals from the restricted range analysis, plotted in red, show little remaining structure. While not shown in this paper, a plot of the periodogram of the residuals from the restricted and unrestricted frequency analyses showed only minor differences.

The eight-stage restricted analysis resulted in a modest reduction in the number of statistically significant frequencies reported in Table 3. Nevertheless, in both cases the number of spurious frequencies reported (27 for the restricted and 36 for the unrestricted) exceeded the number of real frequencies in the data. While raising the significance level would have eliminated some of the spurious frequencies, some were of such high significance—for example, the 22.456008 cycles d^{-1} frequency had a significance of 83.94—that not all spurious frequencies could be eliminated by this method.

Figure 2 gives us an indication of why spurious frequencies are unavoidable. Panel (a) of the Figure is of a frequency with two nearby spurious frequencies while panel (b) has a single significant frequency. In panel (b) the scaled spectral window almost completely obscures the data periodogram. Panel (b) shows that if the pulsation generates a sinusoid in the light curve, there should be no complicating spurious frequencies in its immediate neighborhood. In Panel (a) there are two very distinct deviations in the periodogram from the spectral window, both of relatively high significance (12.25 and 11.60, respectively). While both frequencies are required mathematically to describe the data, when interpreted in terms of a model of stellar pulsations, they would not correspond to any physical pulsation. Without the prior knowledge of the construction of this data set, one would almost certainly accept these frequencies as physically meaningful, and in one sense they are because they give information about the shape of the pulsation.

5.2. EE Cha Data

Attempting a frequency analysis of astronomical light curve data where multiple non-sinusoidal pulsations are present is extremely challenging, as previous literature and the results presented above and in Paper I show. The difference in the number statistically significant frequencies reported by SigSpec and FAMIAS in Table 6 is easily explained by the fact that FAMIAS is limited to 100 frequencies whereas SigSpec does not have this limitation. The difference in the number of reported statistically significant frequencies between the unrestricted and restricted range analysis is quite dramatic even though the analysis was carried out with the same software, namely SigSpec (Reegen 2011).

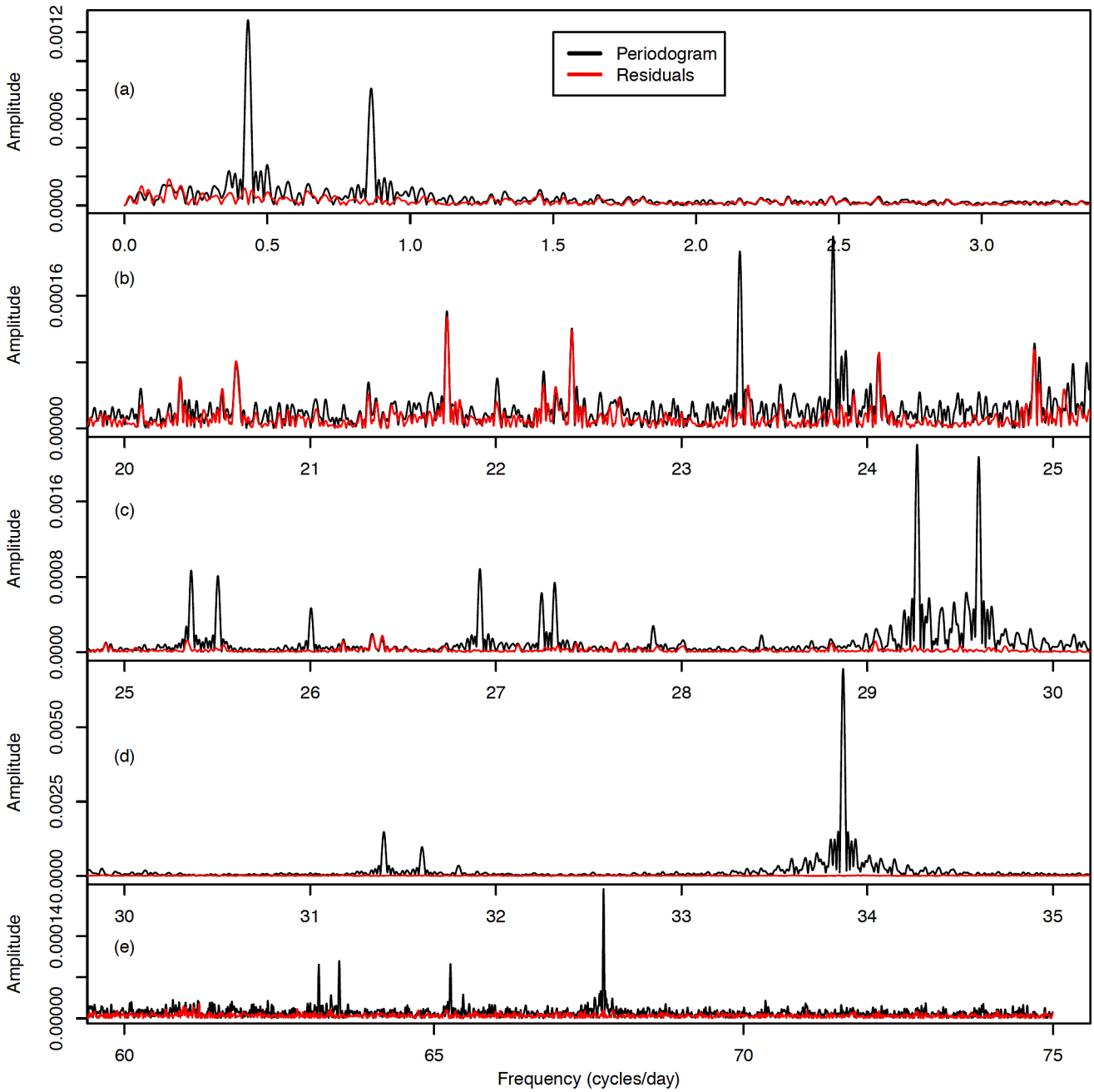

Figure 8. The periodogram of the full two-sector data set is in black while the periodogram of the residuals after the nine-stage restricted range analysis was run is in red. The vertical axis in each of the five panels is not to the same vertical scale.

Although the significance level used was the same in both cases, part of the difference may be because of what is considered signal and what is considered noise in the light curve. A problem familiar to users of FAMIAS (Zima 2008) is that often a frequency is first reported as statistically insignificant but after a few more cycles of pre-whitening it reaches statistical significance. Consider a light curve composed of 10 pulsation frequencies and some noise. After the first cycle of frequency analysis one frequency will have been identified as the strongest and the remaining nine will be grouped with the true noise as just noise. After the second pre-whitening cycle the second strongest frequency will be identified and the remaining eight will be grouped with the true noise as just noise. If the signal-to-noise ratio (SNR) is calculated at each stage, the SNR of the first frequency will increase with each subsequent cycle of pre-whitening and analysis. For example, with only the single 33.869470 cycles d^{-1} frequency included, FAMIAS reported its SNR as 267.80. If all of the frequencies from the restricted range analysis were included, its SNR rose to 323.99.

The periodogram of the residuals from the restricted range frequency analysis in Figure 8 clearly has a lot of remaining structure. Some of that will be artifacts from the analysis, as Balona (2014) and Paper I have shown, but some will likely be from unidentified physically meaningful but weak pulsations. Thus, two things must be done after running a restricted range frequency analysis. The first is to check every statistically

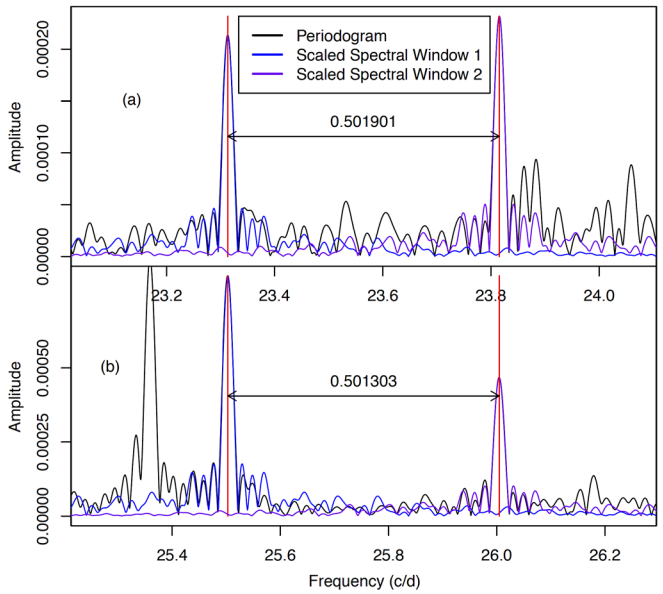

Figure 9. Two doublets with nearly identical spacing from the full two-sector data set. Panel (a) displays frequencies F3 and F4 in Table 7 and panel (b) displays frequencies F6 and F7.

significant frequency against the periodogram to ensure it corresponds to some identifiable feature. Second, the periodogram of the residuals must be examined carefully for evidence of physically meaningful pulsations which may have been missed.

Taking the first of these two steps, of the 32 statistically significant frequency reported by the restricted range analysis, 13 of these had a problem when matched to the periodogram. As illustrated in Figure 7, the two types of problems were, firstly, as in panel a, the identified frequency was close to the local peak of the periodogram but did not match it and, secondly, as in panel b, there was no discernible feature in the periodogram at, or near, the location of the significant frequency. There were four of the first type and nine of the second. At least some of both types appear to be caused by interference from a side lobe of a nearby stronger frequency. In all four cases where the periodogram peak was slightly displaced from the location of the identified frequency, either the second or third side lobe of a nearby strong peak was situated within the frequency span of the peak. Three of the four had significances above 10. The question is whether one should manually correct the reported frequency to match the location of the periodogram peak. This does not appear to be advisable because the side lobe and the real frequency were combined into a single peak in the periodogram. Software such as FAMIAS or SigSpec should be able to disentangle such merged features.

By contrast, all nine frequencies which did not match a discernible feature in the periodogram had significances of less than 7.5. There seems little reason to retain these for they appear to be artifacts of the pre-whitening process, something entirely expected.

Moving now to checking for missed frequencies, Figure 8 compares the periodogram of the residuals from the restricted range analysis (red) with the periodogram of the data (black). Not all of the periodogram is presented; the two long-frequency regions 3–20 and 35–60 cycles d^{-1} are omitted because they appeared to consist of nothing but noise. Panel (a) covers the γ Doradus frequency range and there appears to be no noticeable peaks in the residuals, from which we conclude that the two identified frequencies were all that there are in this region.

In panel b of Figure 8 there appear to be several peaks in the periodogram of both the full data set and in the residuals which do not appear to have been adequately modelled in the restricted range analysis. For example, the peaks at 21.737048 and 22.408476 cycles d^{-1} had significances of 104.78 and 89.64, respectively, in the unrestricted analysis. While not obvious at the vertical scale used in panel b, there are several peaks in the periodogram of the residuals that are larger than the same peaks in the periodogram of the data. This is the result of modelling a non-sinusoidal pulsation with a single sinusoid and some of the power from the pulsation leaking out into other parts of the periodogram in the pre-whitening process.

Similarly, in panel c there appear to be a few frequency peaks missed in the restricted range analysis. These missed frequencies in panels b and c are included as frequencies F23–F30 in Table 7.

In panel d of Figure 8 there appears to be no strong frequency in the residuals, indicating that in this frequency range the few frequencies identified during the restricted range frequency analysis were adequate to model the data.

In panel e of Figure 8 there are a number of peaks in the periodogram of the original data set that do not appear in the residuals, even though only a single statistically significant frequency in the 60–75 cycles d^{-1} range was identified at 67.738708 cycles d^{-1} then modelled and removed. It is likely that these other periodogram peaks are overtones from lower frequencies which, once these lower frequencies were modelled and removed, also removed these apparently strong peaks in the high frequency region.

Once the detailed frequency identification was complete, then the extracted frequencies could be analyzed for information they may provide on the structure of the star. Since this paper is primarily about frequency analysis, we only note two features of the identified frequencies. The first is that frequencies of the form f, 2f, 3f... often indicate an asymmetric pulsation which requires more than one frequency in the Fourier series to adequately model it. Table 8 presents two such groupings. This raises the question of whether the 0.863226 cycle d^{-1} is, in fact, real or the result of an asymmetry in the 0.432322-d^{-1} pulsation. Given the strength of the higher of these two frequencies we might have expected significant frequencies at 3f and 4f. Neither of these frequencies appeared in the unrestricted analysis and there is no evidence of an unmodelled pulsation in the periodogram of the residuals. This implies that the 0.863226 cycle-d^{-1} pulsation was physically meaningful.

The second pair in Table 8 is much more likely to be the result of slight asymmetry in the lower frequency, which is the strongest pulsation in the data. We did not search for a frequency of the form 3f, which would have had a frequency near 100 cycles d^{-1}. However, given the magnitude of the reduction in amplitude of 2f relative to 1f (31.5 to 1), a similar reduction in amplitude between 2f and 3f would have rendered the peak indistinguishable from noise even if it existed.

Figure 9 presents two doublets with nearly the same frequency spacing. The scale of the horizontal axes is the

same in both panels. Rotational splitting of pulsation modes is expected to give rise to a multiplet with an odd number of frequencies. However, as Aerts and Kurtz (2010, p. 16) point out, not all members of the multiplet may be excited to the same amplitude and, consequently, not all members of the multiplet will be observable in the data. With a single published v sin i value of 93 km/s (Royer *et al.* 2002, 2007), the frequency spacing may well reflect the rotational period.

6. Conclusions and suggestions for further research

There appears to be no simple solution to the problem of separating the reported statistically significant frequencies into those which correspond to a pulsation and those which are mathematically required to describe the data (for example because of changes in the amplitude of a pulsation or asymmetric light curve shape) but do not correspond to a pulsation mode. The restricted range analysis proposed in Paper I has the advantage of being particularly simple to implement. Our results suggest the following approach is useful:

1. Run an unrestricted range frequency analysis followed by a restricted range analysis, dividing the frequency range into sub-ranges with visually obvious peaks and sub-ranges which appear to be only noise.

2. Compare all significant frequencies from the restricted range analysis against the data periodogram. Accept each one which matches a distinct feature within it, while making use of the scaled spectral window to examine the effects of a strong frequency on nearby periodogram peaks. Reject those frequencies which do not match any discernible feature in the periodogram.

3. Carefully examine the periodogram of the residuals from the restricted range analysis for unexplained peaks which also appear in the data periodogram. Check these against possible significant frequencies in the unrestricted analysis.

4. After obtaining a set of candidate frequencies, make a search for combination frequencies.

As pointed out above, step 2 is problematic because frequencies which are mathematically necessary to describe the data may have an apparently high significance and easily discernible periodogram feature while corresponding to no physical pulsation in the star of interest.

There are promising new methods proposed to distinguish between mathematically and physically meaningful pulsation frequencies, such as that proposed by Lares-Maritz *et al.* (2020). This and other methods need further research.

Looking towards the future, because EE Cha is a young δ Scuti with a relatively simple periodogram and is relatively bright (Mag 6.7 in V), it would benefit from an intensive spectroscopic observing campaign to attempt to do mode identification.

7. Acknowledgements

The author would like to thank the editor and an anonymous referee who commented on Paper I for valuable comments which helped to improve both papers.

The author would like to thank NASA for making the data from its Transiting Exoplanet Survey Satellite freely available and the TESS Asteroseismic Science Operations Center (TASOC) for operating their particular database of TESS photometry data.

The author would like to thank the American Association of Variable Star Observers for maintaining and making freely available the Variable Star Index (VSX).

This research has made use of the SIMBAD database, operated at CDS, Strasbourg, France.

References

Aerts, C, Christensen-Dalsgaard, J., and Kurtz, D. W. 2010, *Asteroseismology*, Springer Science + Business Media B. V., Dordrecht.

Balona, L. A. 2014, *Mon. Not. Roy. Astron. Soc.*, **439**, 3453.

Catelan, M., and Smith, H. A. 2015, *Pulsating Stars*, Wiley-VCH, Weinheim, Germany.

Gaia Collaboration, *et al.* 2020, *Astron. Astrophys.*, **649A**, 1 (doi:10.5270/esa-1ug).

Grigahcène, A., *et al.* 2010, *Astrophys. J., Lett.*, **713**, L192.

Kurtz, D., and Müller, M. 1999, *Mon. Not. Roy. Astron. Soc.*, **310**, 1071.

Lares-Maritz, M., Garrido, R., and Pascual-Granado, J. 2020, *Mon. Not. Roy. Astron. Soc.*, **498**, 1194.

Murphy, S. J., Lawson, W. A., and Bessell, M. B. 2013, *Mon. Not. Roy. Astron. Soc.*, **435**, 1325.

Poretti, E., *et al.* 2009, *Astron. Astrophys.*, **506**, 85.

R Core Team. 2019, R: A Language and Environment for Statistical Computing, R Foundation for Statistical Computing, Vienna, Austria (https://www.R-project.org).

Rea, B. 2022, *J. Amer. Assoc. Var. Star Obs.*, **50**, 8.

Reegen, P. 2011, *Commun. Asteroseismology*, **163**, 3.

Ricker, G. R., *et al.* 2014, *Proc. SPIE*, **9143**, id. 914320.

Royer, F., Gerbaldi, M., Faraggiana, R., and Gómez, A. E. 2002, *Astron. Astrophys.*, **381**, 105.

Royer, F., Zorec, J., and Gómez, A. E. 2007, *Astron. Astrophys.*, **463**, 671.

Uytterhoeven, K., *et al.* 2011, *Astron. Astrophys.*, **534**, A125.

Wenger, M., *et al.* 2000, *Astron. Astrophys., Suppl. Ser.*, **143**, 9.

Zima, W. 2008, *Commun. Asteroseismology*, **155**, 17.